Journal of Materials Chemistry A

ROYAL SOCIETY OF CHEMISTRY

PAPER

View Article Online
View Journal | View Issue

Cite this: J. Mater. Chem. A, 2025, 13, 22924

Multicomponentization of a super-Na ionic conductor chloride $NaTaCl_6$, enhancing ionic conductivity and electronic resistivity†

Keisuke Makino,[a] Naoto Tanibata, *[a] Takaaki Natori,[b] Tomoko Nakano,[b] Hayami Takeda [a] and Masanobu Nakayama [a]

All-solid-state Na-ion batteries have attracted considerable attention because of their advantages such as high safety, high energy density, and low cost. Solid electrolytes used in these batteries require high Na-ion conductivity to minimize energy loss, high electronic resistivity to prevent self-discharge, and high oxidation resistance to enable the use of high-potential cathodes. Recently, $NaTaCl_6$ was reported to possess both high oxidation resistance and ionic conductivity, and its ionic conductivity improved with a decrease in its crystallinity. Therefore, in this study, we aimed to further reduce the crystallinity of $NaTaCl_6$ and improve its ionic conductivity and electronic resistivity through multicomponentization. The verified composition was $Na_2Ta_{0.625}Zr_{0.25}Ga_{0.125}Cl_{5.625}(CO_3)_{0.25}(BO_3)_{0.125}$, wherein polyatomic anions (CO_3^{2-} and BO_3^{3-}) were expected to have inductive effects that maintained the high oxidation resistance of chloride. Through multicomponentization, the $NaTaCl_6$ phase transitioned to a low-crystallinity state, resulting in a significant improvement in the ionic conductivity (1.2×10^{-3} S cm^{-1}), which was approximately ten times higher than that of crystalline $NaTaCl_6$ (1.1×10^{-4} S cm^{-1}). The electronic resistivity of the low-crystallinity multicomponent was more than one order of magnitude higher than that of crystalline $NaTaCl_6$, effectively suppressing self-discharge and improving the energy-storage preservation properties of the material. Furthermore, the multicomponent $NaTaCl_6$ retained a high oxidation resistance with an oxidation limit of 4.6 V *vs.* Na/Na^+. Thus, this multicomponentization strategy simultaneously retains high oxidation resistance while improving the ionic conductivity and electronic resistivity of the electrolyte material, thereby enabling the development of high-performance all-solid-state Na-ion batteries.

Received 28th November 2024
Accepted 11th March 2025

DOI: 10.1039/d4ta08447k

rsc.li/materials-a

Introduction

Owing to their high energy density, Li-ion batteries are widely used in various applications, including cell phones and electric vehicles (EVs).[1] However, conventional Li-ion batteries employ flammable liquid organic electrolytes, which can occasionally lead to explosions and other safety concerns.[2] To address these issues, all-solid-state batteries, in which liquid electrolytes are replaced with nonflammable solid electrolytes, have gained considerable attention because of their improved safety.[3] However, as the demand for Li continues to grow with the shift from conventional vehicles to EVs, the cost of Li-based materials is expected to increase.[4] Consequently, Na-based batteries have recently attracted interest as promising alternatives because of the abundance of Na on Earth.[5] As a base alkali metal similar to Li, Na offers the potential for developing low-cost Na-ion batteries.[6] Therefore, Na-ion all-solid-state batteries, which have the advantages of safety, high energy density, and low cost, have been the focus of extensive research.[7] Further, a solid electrolyte material with high oxidation resistance is essential for developing high-potential cathodes, which are critical for achieving high energy density in all-solid-state batteries.[8,9] Sulfide-based electrolytes, which are known for their higher ionic conductivity attributed to the greater polarizability of their carrier-ion counterions compared to those of oxides, have been the focus of intensive material development.[10–13] However, sulfide materials typically exhibit relatively low oxidation resistance (~2 V *vs.* Na/Na^+).[14] In contrast, chlorides have recently attracted attention because of their high ionic conductivity, which can be attributed to their high polarizability, and their oxidation resistance, which can be attributed to their high electronegativity.[15–17] A recent study[18] reported that a low crystallinity $NaTaCl_6$ solid electrolyte demonstrated a high ionic conductivity (4.0×10^{-3} S cm^{-1}) at 25 °C along with a high oxidation resistance (4.1 V *vs.* Na/Na^+). The ionic conductivity of

[a]Department of Advanced Ceramics, Nagoya Institute of Technology, Nagoya, Aichi 466-8555, Japan. E-mail: tanibata.naoto@nitech.ac.jp
[b]Toagosei Co., Ltd, Nagoya Criatio R&D Center, 8, Showa-cho, Minato-ku, Nagoya, Japan

† Electronic supplementary information (ESI) available. See DOI: https://doi.org/10.1039/d4ta08447k

this material increased with extended ball milling, which simultaneously reduced its crystallinity and led to blackening. This blackening was likely caused by the formation of a high concentration of defects associated with the prolonged ball-milling process. This ionic conductivity is higher compared to previously reported values for crystalline chloride materials, such as $Na_{3-x}Er_{1-x}Zr_xCl_6$ (3.5×10^{-5} S cm^{-1}),[19] $Na_{3-x}Y_{1-x}Zr_xCl_6$ (6.6×10^{-5} S cm^{-1}),[20] $Na_{2+x}Zr_{1-x}In_xCl_6$ (2.7×10^{-5} S cm^{-1}),[21] Na_2ZrCl_6 (1.8×10^{-5} S cm^{-1} (ref. 22)), $NaAlCl_4$ ($\sim 10^{-5}$ S cm^{-1} (ref. 23)), and $Na_{1-x}Zr_xLa_{1-x}Cl_4$ (2.9×10^{-4} S cm^{-1} (ref. 24)).

We performed a multicomponent modification of the chloride solid electrolyte $NaTaCl_6$ to further improve its ionic conductivity while maintaining its high oxidation resistance. Our approach focused on developing low-crystallinity compounds with a high Na^+ concentration by substituting multiple elements for the cation (Ta^{5+}) and anion (Cl^-). The multicomponentization of the system was expected to stabilize the low-crystallinity state.[25,26] The mixed-anion effect, which improves ionic conductivity, is a well-known phenomenon attributed to anion complexation within amorphous structures.[27] In addition, the ionic conductivity in the amorphous structures increases exponentially with the carrier ion concentration,[28] suggesting that increasing the Na concentration through charge compensation associated with elemental substitution can significantly enhance ionic conductivity. Ta^{5+} ($r = 0.64$ nm; 6-coordination), Zr^{4+} ($r = 0.72$ nm; 6-coordination), and Ga^{3+} ($r = 0.62$ nm; 6-coordination)[29] were selected as cation substitutes. These elements have a lower valence than pentavalent Ta^{5+} but possess similar ionic radii. For the anion substitution of Cl^-, ions with valences higher than those of monovalent Cl^- were necessary for increasing the Na concentration. However, a key challenge is that monatomic ions with higher valences than Cl^- (such as S^{2-} and P^{3-}) can undergo oxidation at low potentials,[30] which would loses the high oxidation resistance typical of chlorides. Thus, polyatomic anions with a thermodynamic radius r_H similar to that of Cl^- ($r = 1.81$ nm),[29] specifically CO_3^{2-} ($r_H = 1.78$ nm), and BO_3^{3-} ($r_H = 1.91$ nm),[31] were selected. These anions were selected because of their high resistance to oxidation, which is attributed to the inductive effect [32] of their highly electronegative cations (C^{4+} and B^{3+}). Furthermore, energy storage preservation performance is a critical parameter in batteries.[33,34] Although Li-ion batteries are known for their lower self-discharge and superior energy storage preservation performance compared to those of other systems such as Ni-metal hydride batteries,[35] the use of solid electrolytes often characterized by lower electronic resistivity than that of liquid electrolytes raises concerns about potential self-discharge caused by electronic conduction in the solid electrolyte. The low electronic resistivity of solid electrolytes can promote the growth of metal dendrites, thereby leading to short-circuiting and eventual cell failure.[36] Reducing the crystallinity of a material increases its electrical resistivity.[37] We aimed to achieve low electronic conductivity, which can improve battery storage properties by inducing low crystallinity through the multicomponentization of the system.

In this study, we explored the incorporation of multiple components into the highly ionically conductive $NaTaCl_6$ chloride to simultaneously enhance its ionic conductivity and electronic resistivity while maintaining its high oxidation resistance. To achieve multicomponentization, Zr^{4+}, Ga^{3+}, CO_3^{2-}, and BO_3^{3-} were selected as the substituted species for the aforementioned reasons.

Results and discussion

The composition of multicomponent $NaTaCl_6$ was determined to be $Na_2Ta_{0.625}Zr_{0.25}Ga_{0.125}Cl_{5.625}(CO_3)_{0.25}(BO_3)_{0.125}$ (Na–Ta–Zr–Ga–Cl–CO_3–BO_3), with equal amounts of cations and anions substitution. The substituted species with valences closes to those of the original ion were used to double the amount to ensure a nominal Na composition of 2. Fig. 1(a) shows the X-ray diffraction (XRD) patterns of $NaTaCl_6$ and Na–Ta–Zr–Ga–Cl–CO_3–BO_3 synthesized *via* a mechanochemical method using a ball mill. The $NaTaCl_6$ crystal peak is visible in the unsubstituted $NaTaCl_6$, whereas the $NaTaCl_6$ crystal peak is almost absent in the multicomponent Na–Ta–Zr–Ga–Cl–CO_3–BO_3, indicating the successful formation of a low-crystallinity compound through multicomponentization. Most $NaTaCl_6$ peaks disappeared in this material, and therefore, the major phase appeared to be amorphous. However, some low-intensity crystalline peaks corresponding to $NaTaCl_6$ remain. Furthermore, the Na–Ta–Zr–Ga–Cl–CO_3–BO_3 composition exceeded the solid solubility limit of Na, as evidenced by the presence of an impurity peak corresponding to NaCl. These observations confirm that this material is a glass-ceramic composite composed of the amorphous phase of the main component with low-crystallinity $NaTaCl_6$ and crystalline NaCl as impurities. Although determining the optimum composition remains a task for future studies, we successfully synthesized a low-crystallinity compound, which was the primary goal of this study. Further analysis was performed on samples with this composition, and photographs of the samples are shown in Fig. 1(b and c). Unlike the previously reported low-crystallinity $NaTaCl_6$, which exhibited black discoloration,[18] Na–Ta–Zr–Ga–Cl–CO_3–BO_3 synthesized in this study retained its white color, similar to that of crystalline $NaTaCl_6$.

The Raman spectra of $NaTaCl_6$ and Na–Ta–Zr–Ga–Cl–CO_3–BO_3 are shown in Fig. 1(d and e), respectively. The low-Raman shift peak at $\sim$400 cm^{-1}, indicated by the black circle in Fig. 1(d), appears at a lower position for Na–Ta–Zr–Ga–Cl–CO_3–BO_3 compared with the corresponding peak for $NaTaCl_6$. According to Ohno *et al.*,[38] in $Na_{1+x}Ta_{1-x}Zr_xCl_6$ (where $NaTaCl_6$ is doped with Zr), the $[TaCl_6]^-$ peak shifts toward lower Raman shifts with an increase in the amount of Zr doping (x). Thus, the shift of the black circular peak to a lower Raman shift in this study could likely be attributed to Zr and Ga doping. In addition, for Na–Ta–Zr–Ga–Cl–CO_3–BO_3, the black circular peak broadened because of the low crystallinity of the $NaTaCl_6$ phase. Further, several shoulder peaks appeared on the lower Raman shift side of the black circular peak; this was not observed for $NaTaCl_6$, which was attributed to contributions from the $[GaCl_6]^{3-}$ and $[ZrCl_6]^{2-}$ peaks.[38] The peaks observed near 900 cm^{-1} (red circle) and 1100 cm^{-1} (black circle) in Fig. 1(e) are attributed to the BO_3^{3-} unit [39] and CO_3^{2-} unit,[40] respectively,

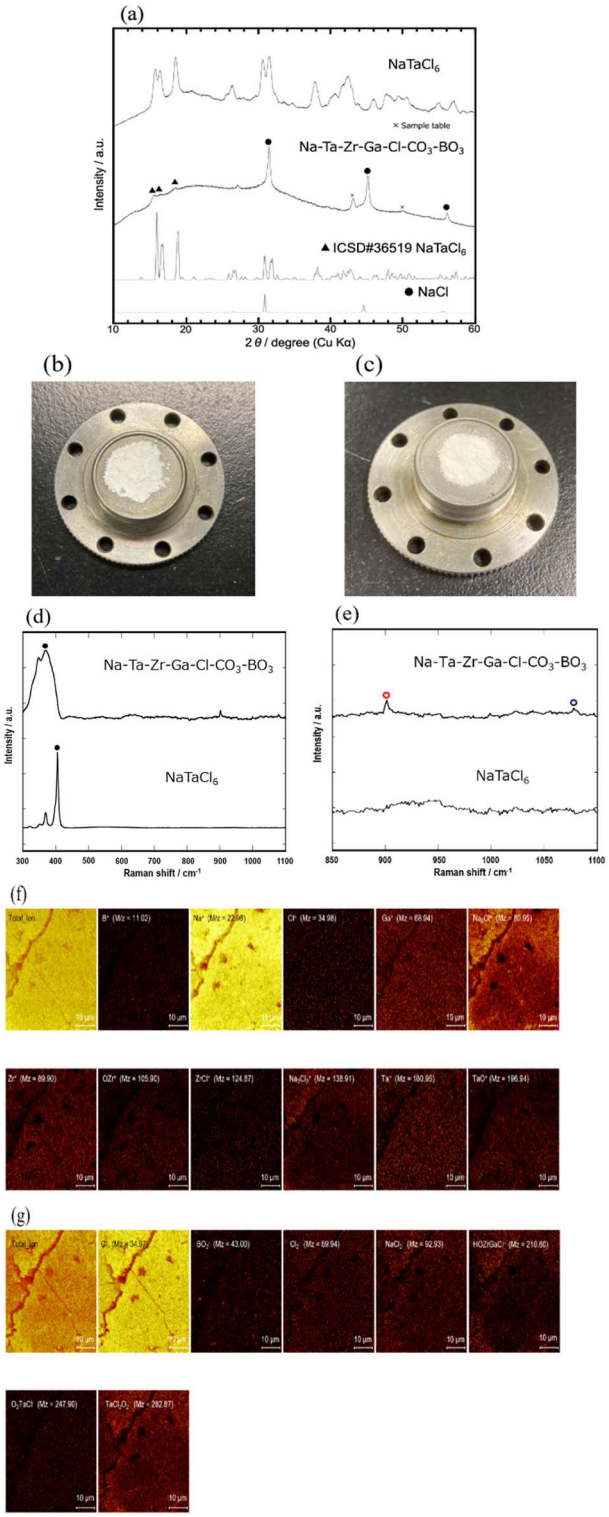

Fig. 1 Characterization results for mechanically synthesized $NaTaCl_6$ and Na–Ta–Zr–Ga–Cl–CO_3–BO_3. (a) XRD patterns of $NaTaCl_6$ and Na–Ta–Zr–Ga–Cl–CO_3–BO_3. (b and c) Photographs of the synthesized powder samples of $NaTaCl_6$ and Na–Ta–Zr–Ga–Cl–CO_3–BO_3, respectively. (d and e) Raman spectroscopy results; (d) shows a general view of the measurement range, and (e) presents a magnified view of the Raman shift range between 850 and 1100 cm^{-1}. (f and g) TOF-SIMS measurement results on the pellet surface of Na–Ta–Zr–Ga–Cl–CO_3–BO_3, showing ion mapping of cations and anions, respectively.

thereby confirming the presence of these polyatomic anion units without decomposition. Further, we performed time-of-flight secondary ion mass spectrometry (TOF-SIMS) measurements, which showed high spatial resolution even for such insulating samples, to observe the dispersion of these units.[41] The TOF-SIMS spectra are shown in Fig. S1(a and b),† which primarily display signals attributed to the units of each cation (Na, Ta, Zr, Ga, and B) and anion (Cl and O). The spatial distributions of these ions are shown in Fig. 1(f and g), which indicate that all constituent elements, except for the CO_3 unit, are uniformly present at the submicrometer scale. The absence of the CO_3 unit is likely caused by its tendency to desorb as CO_2 during TOF-SIMS measurements. The Cole–Cole plots from the AC impedance measurements for $NaTaCl_6$ and Na–Ta–Zr–Ga–Cl–CO_3–BO_3 at various temperatures are shown in Fig. 2(a and b), respectively. The shape of the Cole–Cole plots shows a partial semicircle on the high-frequency side, along with a slope on the low-frequency side attributed to the ion-blocking electrode, thereby indicating that the resistance of the semicircle is caused by ionic conduction. Although both bulk and grain boundary resistances were expected for the pressed powder samples, they could not be individually distinguished from the plots. Therefore, the total resistance (sum of the bulk and grain boundary resistances) was considered in the evaluation of ionic conductivity. The total ionic conductivities were calculated using the resistance values indicated by the black arrows in the plots. The ionic conductivity of Na–Ta–Zr–Ga–Cl–CO_3–BO_3 (1.2×10^{-3} S cm^{-1}) was approximately ten times higher than that of $NaTaCl_6$ (1.1×10^{-4} S cm^{-1}), despite the presence of NaCl as an

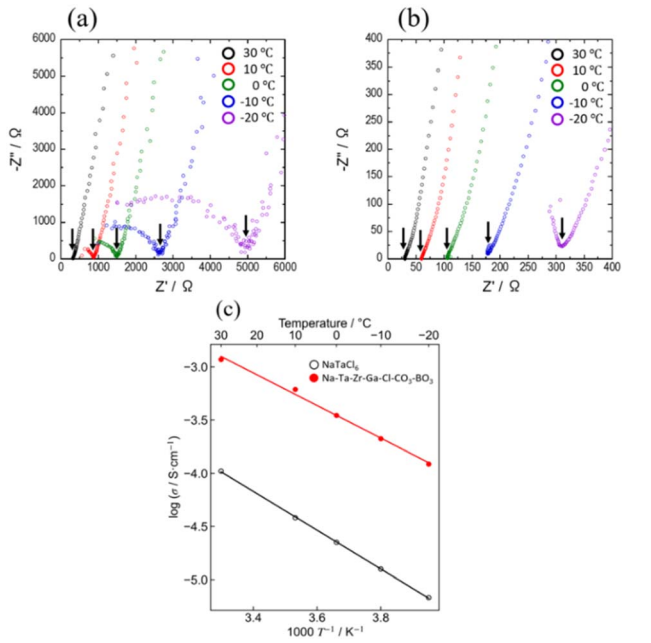

Fig. 2 AC impedance measurements of $NaTaCl_6$ and Na–Ta–Zr–Ga–Cl–CO_3–BO_3. (a and b) Cole–Cole plots for $NaTaCl_6$ and Na–Ta–Zr–Ga–Cl–CO_3–BO_3 at various temperatures, respectively. (c) Arrhenius plot derived from these results, when black open circles and red filled circles indicate $NaTaCl_6$ and Na–Ta–Zr–Ga–Cl–CO_3–BO_3, respectively.

impurity. The ionic conductivity of the components (terminal compounds) added in this study is low (Na_2ZrCl_6; 1.8 × 10^{-5} S cm^{-1},[42] Na_3BO_3; 1.5 × 10^{-8} S cm^{-1},[43] *etc.*), and this improvement in ionic conductivity can be achieved because of the multicomponent nature of the material. Scanning electron microscopy (SEM) images of the cross sections of the $NaTaCl_6$ and Na–Ta–Zr–Ga–Cl–CO_3–BO_3 pellets (Fig. S2(a and b),† respectively) show that the grain boundaries nearly disappeared in both samples after cold pressing, suggesting that even the multicomponent material retained the high deformability derived from chloride,[44,45] and that the grain boundary resistance has a minimal impact on these materials. The Arrhenius plot in Fig. 2(c) revealed that the activation energy of low-crystallinity Na–Ta–Zr–Ga–Cl–CO_3–BO_3 was 0.30 eV, which is lower than that of crystalline $NaTaCl_6$ (0.36 eV). This decrease in the activation energy indicates that the potential landscape for the carrier ions is smoothed by the effects described above.

The results of the DC polarization tests (Fig. 3) provide valuable insights into the electronic resistivity of $NaTaCl_6$ and the multicomponent Na–Ta–Zr–Ga–Cl–CO_3–BO_3 system. The electronic resistivity calculated from the steady-state current values was found to be 6.7 × 10^9 Ω cm for $NaTaCl_6$ and 1.2 × 10^{10} Ω cm for Na–Ta–Zr–Ga–Cl–CO_3–BO_3. These values suggest that electronic resistivity increased by approximately twofold after multicomponentization of the material. The rapid relaxation of the current values observed in the initial phase of the test for both samples was attributed to the polarization of ions, which likely resulted from the high ionic conductivity of the materials. Notably, this relaxation rate was faster in Na–Ta–Zr–Ga–Cl–CO_3–BO_3, which was consistent with its higher ionic conductivity compared to that of $NaTaCl_6$.

Fig. 4 shows the linear sweep voltammetry (LSV) results for $NaTaCl_6$ and Na–Ta–Zr–Ga–Cl–CO_3–BO_3. The slight difference between these plots suggests that the high oxidation resistance derived from chloride was retained even with the substitution of polyatomic anions (CO_3^{2-} and BO_3^{3-}). The larger current values in Na–Ta–Zr–Ga–Cl–CO_3–BO_3 compared to those in $NaTaCl_6$ may be attributed to the higher ionic conductivity of Na–Ta–Zr–Ga–Cl–CO_3–BO_3. First-principles calculations were performed to validate oxidation limits. Data for $NaTaCl_6$, obtained from the Materials Project, an inorganic material database, were used as the original cell structure for these calculations. The number of

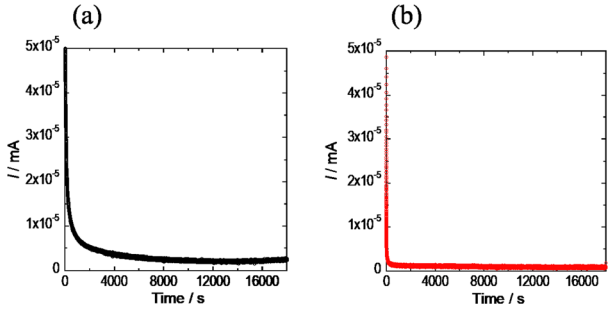

Fig. 3 Results of DC polarization tests. (a) $NaTaCl_6$ and (b) Na–Ta–Zr–Ga–Cl–CO_3–BO_3.

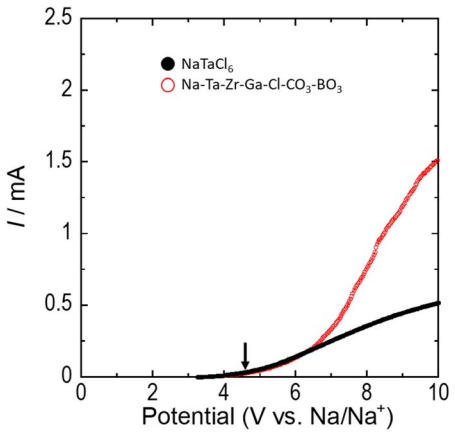

Fig. 4 LSV results. The black and red circles indicate the middle outliers for $NaTaCl_6$ and Na–Ta–Zr–Ga–Cl–CO_3–BO_3, respectively. The cell configuration used in the measurements was $Na_{10}Sn_4$ (ref. 46)|Na_3PS_4|$NaTaCl_6$|measurement sample + KB.

atoms in the cell was set to 32, and the oxidation limit potential was calculated based on the energy difference between the original composition and the composition without Na atoms. Na desorption model calculations indicated an oxidation limit of 4.6 V *vs.* Na/Na^+ for $NaTaCl_6$. The thermodynamic oxidation limit was investigated by extracting the compositional data of the decomposition components from the Materials Project and performing convex-hull calculations for these components. Details of the calculations are provided in the ESI.† The oxidation limit determined using the convex-hull model calculation was determined to be 3.6 V *vs.* Na/Na^+. The oxidation of the material is expected to cause decomposition through the reaction $NaTaCl_6 \rightarrow Na + TaCl_5 + 1/2Cl_2$. The oxidation limits for $NaTaCl_6$ and Na–Ta–Zr–Ga–Cl–CO_3–BO_3 are estimated to be 4.6 V *vs.* Na/Na^+ based on Fig. 4. This value was consistent with the results of the Na desorption model calculations. These findings suggest that the reaction predicted by the convex-hull model calculations was not observed in the actual LSV measurements because of the high resistance caused by significant structural changes. In addition, these oxidation limits (4.6 V *vs.* Na/Na^+) are higher than the oxidation limit reported by Hu *et al.* for $NaTaCl_6$ (4.1 V *vs.* Na/Na^+).[18] One possible reason for this discrepancy is the black discoloration of the $NaTaCl_6$ sample.

Fig. 5 compares the performance of the materials obtained in this study ($NaTaCl_6$ and Na–Ta–Zr–Ga–Cl–CO_3–BO_3) with those of representative Na-ion-conductive chlorides, sulfides, selenides, and oxides ($Na_{2.88}Sb_{0.88}W_{0.12}S_4$,[47] Na_3PS_4,[48] $Na_{11}Sn_2PS_{12}$,[49] $Na_3Zr_2Si_2PO_{12}$,[50,51] Na_3PSe_4,[52] $Na_{3-x}Y_{1-x}Zr_xCl_6$,[20] $Na_{2.5}Cr_{0.5}Zr_{0.5}Cl_6$,[53] Na_2ZrCl_6,[22] $NaAlCl_4$,[23] $NaTaCl_6$ (black)[18]). The ionic conductivities and electronic resistivities are shown in Fig. 5(a) and Table S1.† Na–Ta–Zr–Ga–Cl–CO_3–BO_3 obtained in this study exhibited superior ionic conductivity and higher electronic resistivity than the other chlorides, with relatively high values.

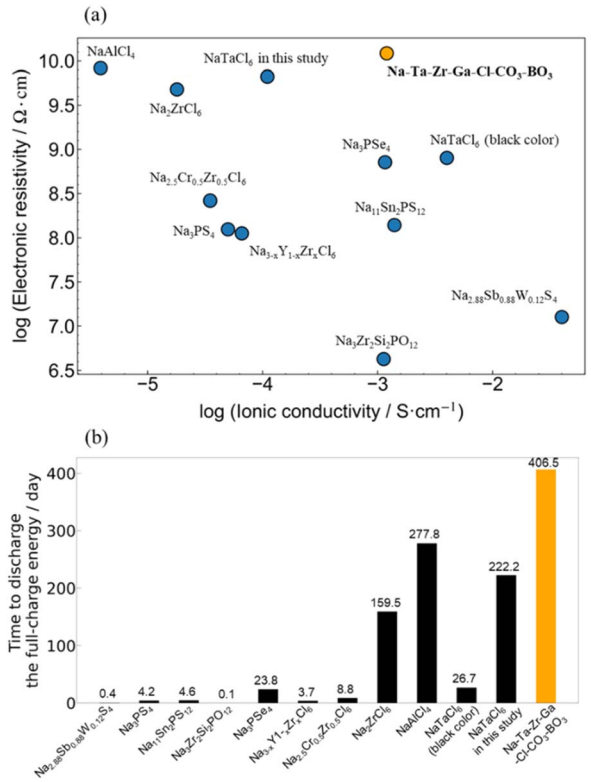

Fig. 5 Comparison of the performance of the materials obtained in this study ($NaTaCl_6$ and Na–Ta–Zr–Ga–Cl–CO_3–BO_3) with representative Na-ion conductive materials ($Na_{2.88}Sb_{0.88}W_{0.12}S_4$,[47] Na_3PS_4,[48] $Na_{11}Sn_2PS_{12}$,[49] $Na_3Zr_2Si_2PO_{12}$,[50,51] Na_3PSe_4,[52] $Na_{3-x}Y_{1-x}Zr_xCl_6$,[20] $Na_{2.5}Cr_{0.5}Zr_{0.5}Cl_6$,[53] Na_2ZrCl_6,[22] $NaAlCl_4$,[23] $NaTaCl_6$ (black color)[18]). (a) Axes show the logarithm of ionic conductivity *versus* the logarithm of electronic resistivity. (b) Comparison of the time until complete energy loss from a full charge occurs due to leakage current, derived from the electronic resistivity of the electrolyte. This time is calculated using the electronic conduction resistance of the electrolyte layer and the leakage current value, determined by Ohm's law from a typical battery voltage of 3 V.

In addition, to demonstrate the effectiveness of this high electronic resistivity, we estimated the time required for complete energy loss caused by self-discharge using the leakage current value calculated from the electronic conduction resistance of the electrolyte layer and Ohm's law based on the voltage of a typical battery (3 V). This calculated time is likely to be underestimated, as energy losses can occur because of factors such as reactions between the electrode and electrolyte. Assumed parameters,[54] such as battery capacity (1.2 mA h cm^{-2}) and electrolyte thickness (20 μm), are summarized in Table S2†. Fig. 5(b) compares these results with those of representative Na-ion-conductive materials.

Sulfides tend to have higher electronic conductivity than chlorides. In this hypothetical experiment, the time to lose energy from a full charge, calculated from the electronic conductivity of the sulfide showing the highest Na-ion conductivity ($Na_{2.88}Sb_{0.88}W_{0.12}S_4$), was within half a day (0.4 d). However, chlorides exhibit a low electronic conductivity, which increases the time required for energy loss. However, the previously reported black $NaTaCl_6$ (ref. 18) lost its fully charged energy in approximately one month (26.7 days). It has been suggested that an electronic conductivity of approximately 10^{-10} S cm^{-1} or lower is required to preserve energy storage properties for more than six months.

In this study, we successfully reduced the crystallinity of $NaTaCl_6$ while maintaining its white color and significantly extended the time required for complete energy loss from full charging. Specifically, through multicomponentization, the time to discharge the full-charge energy exceeded 13 months (406.5 d). This result indicated that the multicomponentization approach used in this study effectively enhanced the energy-storage preservation characteristics by suppressing the self-discharge of the battery.

Conclusion

In this study, a multicomponentization strategy was employed by substituting several elements to reduce the crystallinity of $NaTaCl_6$, which exhibits excellent ionic conductivity in a low crystallinity state. This strategy produced a system with low crystallinity, resulting in a ten-fold increase in ionic conductivity ($NaTaCl_6$: 1.1×10^{-4} S cm^{-1}, Na–Ta–Zr–Ga–Cl–CO_3–BO_3: 1.2×10^{-3} S cm^{-1}). This improvement can be attributed to the combined effects of the mixed anions[27] and increased Na concentration,[28] in addition to the low crystallinity of the system. Furthermore, the electronic resistivity increased because of the low crystallinity of the system ($NaTaCl_6$: 6.7×10^9 Ω cm, Na–Ta–Zr–Ga–Cl–CO_3–BO_3: 1.2×10^{10} Ω cm), which suppressed self-discharge and resulted in high energy-storage preservation properties (more than 400 days from full charge to complete energy loss in a hypothetical test within a standard single cell) when applied as the solid electrolyte in all-solid-state batteries. Furthermore, despite multiple elemental substitutions, the material retained the high oxidation resistance derived from chloride, suggesting the possibility of stable battery operation even with a high-potential cathode. Therefore, the low crystallinity achieved through multicomponent substitution in chloride electrolytes maintains a high chloride-derived oxidation resistance while improving ionic conductivity and electronic resistivity. This is a successful example of an effective strategy for enhancing the performance of solid electrolytes.

Data availability

All relevant data are available from the corresponding author on reasonable request.

Author contributions

Conceptualization, N. T.; data curation, K. M. and N. T.; formal analysis, K. M.; funding acquisition, N. T. and M. N.; investigation, K. M.; methodology, N. T.; project administration, N. T.; resources, T. N. and T. N.; software, M. N.; supervision, N. T.; validation, K. M.; visualization, K. M.; writing—original draft preparation, K. M. and N. T.; writing—review and editing,

K. M., N. T., and M. N. All authors have read and agreed to the published version of the manuscript.

Conflicts of interest

The authors declare no competing financial interests.

Acknowledgements

This study was partially supported by Grants-in-Aid for Scientific Research (grant numbers 24K01157, 24K17755, and 24H02203) from the Ministry of Education, Culture, Sports, Science, and Technology (MEXT), Japan, a CREST grant from the Japan Science and Technology Agency, Japan (grant number JPMJCR21O6), the Data Creation and Utilization-Type Material Research and Development Project (grant number JPMXP1122712807) from MEXT, and the Fujikura Foundation. We thank Editage for editing and reviewing the manuscript for English language. Part of this study was conducted at the Nagoya Institute of Technology and supported by the Advanced Research Infrastructure for Materials and Nanotechnology (JPMXP1224NI1108) of MEXT, Japan.

Notes and references

1 R. Van Noorden, *Nature*, 2014, **507**, 26–28.
2 L. Han, L. Wang, Z. Chen, Y. Kan, Y. Hu, H. Zhang and X. He, *Adv. Funct. Mater.*, 2023, **33**, 2300892.
3 A. Banerjee, X. Wang, C. Fang, E. A. Wu and Y. S. Meng, *Chem. Rev.*, 2020, **120**, 6878–6933.
4 K. Kubota, M. Dahbi, T. Hosaka, S. Kumakura and S. Komaba, *Chem. Rec.*, 2018, **18**, 459–479.
5 H. L. Yang, B. W. Zhang, K. Konstantinov, Y. X. Wang, H. K. Liu and S. X. Dou, *Adv. Energy Sustainability Res.*, 2021, **2**, 2000057.
6 N. Yabuuchi, K. Kubota, M. Dahbi and S. Komaba, *Chem. Rev.*, 2014, **114**, 11636–11682.
7 N. Tanibata, M. Deguchi, A. Hayashi and M. Tatsumisago, *Chem. Mater.*, 2017, **29**, 5232–5238.
8 J. Liu, S. Wang, Y. Kawazoe and Q. Sun, *ACS Mater. Lett.*, 2023, **5**, 1009–1017.
9 N. Tanibata, S. Takimoto, S. Aizu, H. Takeda and M. Nakayama, *J. Mater. Chem. A*, 2022, **10**, 20756–20760.
10 M. V. Reddy, C. M. Julien, A. Mauger and K. Zaghib, *Nanomaterials*, 2020, **10**, 1606.
11 J. Gu, Z. Liang, J. Shi and Y. Yang, *Adv. Energy Mater.*, 2023, **13**, 2203153.
12 J. Wu, L. Shen, Z. Zhang, G. Liu, Z. Wang, D. Zhou, H. Wan, X. Xu and X. Yao, *Electrochem. Energy Rev.*, 2021, **4**, 101–135.
13 N. Tanibata, M. Kato, S. Takimoto, H. Takeda, M. Nakayama and H. Sumi, *Adv. Energy Sustainability Res.*, 2020, **1**, 2000025.
14 H. Su, Z. Jiang, Y. Liu, J. Li, C. Gu, X. Wang, X. Xia and J. Tu, *Energy Mater.*, 2022, **2**, 200005–200042.
15 R. S. Mulliken, *J. Chem. Phys.*, 1934, **2**, 782–793.
16 Z. Wei, L. F. Nazar and J. Janek, *Batteries Supercaps*, 2024, **7**, e202400005.
17 N. Tanibata, S. Takimoto, K. Nakano, H. Takeda, M. Nakayama and H. Sumi, *ACS Mater. Lett.*, 2020, **2**, 880–886.
18 Y. Hu, J. Fu, J. Xu, J. Luo, F. Zhao, H. Su, Y. Liu, X. Lin, W. Li, J. T. Kim and X. Hao, *Matter*, 2024, **7**, 1018–1034.
19 R. Schlem, A. Banik, M. Eckardt, M. Zobel and W. G. Zeier, *ACS Appl. Energy Mater.*, 2020, **3**, 10164–10173.
20 E. A. Wu, S. Banerjee, H. Tang, P. M. Richardson, J. M. Doux, J. Qi, Z. Zhu, A. Grenier, Y. Li, E. Zhao and G. Deysher, *Nat. Commun.*, 2021, **12**, 1256.
21 T. Zhao, A. N. Sobolev, R. Schlem, B. Helm, M. A. Kraft and W. G. Zeier, *ACS Appl. Energy Mater.*, 2023, **6**, 4334–4341.
22 H. Kwak, J. Lyoo, J. Park, Y. Han, R. Asakura, A. Remhof, C. Battaglia, H. Kim, S. T. Hong and Y. S. Jung, *Energy Storage Mater.*, 2021, **37**, 47–54.
23 J. Park, J. P. Son, W. Ko, J. S. Kim, Y. Choi, H. Kim, H. Kwak, D. H. Seo, J. Kim and Y. S. Jung, *ACS Energy Lett.*, 2022, **7**, 3293–3301.
24 C. Fu, Y. Li, W. Xu, X. Feng, W. Gu, J. Liu, W. Deng, W. Wang, A. M. Abeykoon, L. Su and L. Zhu, *Nat. Commun.*, 2024, **15**, 4315.
25 J. Jiang, Z. Lu, J. Shen, T. Wada, H. Kato and M. Chen, *Nat. Commun.*, 2021, **12**, 3843.
26 A. Pradel and M. Ribes, *Mater. Chem. Phys.*, 1989, **23**, 121–142.
27 B. Carette, M. Ribes and J. L. Souquet, *Solid State Ionics*, 1983, **9–10**, 735–737.
28 C. Ho, I. D. Raistrick and R. A. Huggins, *J. Electrochem. Soc.*, 1980, **127**, 343.
29 R. Shannon, *Acta Crystallogr.*, 1976, **32**, 751–767.
30 S. Zhang, J. Ma, S. Dong and G. Cui, *Electrochem. Energy Rev.*, 2023, **6**, 4.
31 A. F. Kapustinskii, *Q. Rev., Chem. Soc.*, 1956, **10**, 283–294.
32 M. Saubanère, M. B. Yahia, S. Lebègue and M.-L. Doublet, *Nat. Commun.*, 2014, **5**, 5559.
33 M. R. Palacín and A. de Guibert, *Science*, 2016, **351**, 1253292.
34 W. M. Seong, K. Y. Park, M. H. Lee, S. Moon, K. Oh, H. Park, S. Lee and K. Kang, *Energy Environ. Sci.*, 2018, **11**, 970–978.
35 S. H. Choi, J. Kim and Y. S. Yoon, *J. Power Sources*, 2004, **138**, 283–287.
36 F. Han, A. S. Westover, J. Yue, X. Fan, F. Wang, M. Chi, D. N. Leonard, N. J. Dudney, H. Wang and C. Wang, *Nat. Energy*, 2019, **4**, 187–196.
37 H.-X. Deng, S.-H. Wei, S.-S. Li, J. Li and A. Walsh, *Phys. Rev. B:Condens. Matter Mater. Phys.*, 2013, **87**, 125203.
38 Z. Huang, S. Yoshida, H. Akamatsu, K. Hayashi and S. Ohno, *ACS Mater. Lett.*, 2024, **6**, 1732–1738.
39 K. Suzuki, Y. Nakamura, N. Tanibata, A. Hayashi and M. Tatsumisago, *J. Asian Ceram. Soc.*, 2015, **4**, 6–10.
40 N. Buzgar and A. Apopei, *Anal. St. Univ. 'Al. Cuza', Iasi*, 2009, 97–112.
41 T. Lombardo, F. Walther, C. Kern, Y. Moryson, T. Weintraut, A. Henss and M. Rohnke, *J. Vac. Sci. Technol., A*, 2023, **41**, 053207–053222.
42 H. Kwak, J. Lyoo, J. Park, Y. Han, R. Asakura, A. Remhof, C. Battaglia, H. Kim, S. T. Hong and Y. S. Jung, *Energy Storage Mater.*, 2021, **37**, 47–54.

43 K. Suzuki, Y. Nakamura, N. Tanibata, A. Hayashi and M. Tatsumisago, *J. Asian Ceram. Soc.*, 2016, **4**, 6–10.
44 N. Tanibata, N. Nonaka, K. Makino, H. Takeda and M. Nakayama, *Sci. Rep.*, 2024, **14**, 2703.
45 N. Tanibata, S. Aizu, M. Koga, H. Takeda, R. Kobayashi and M. Nakayama, *J. Mater. Chem. A*, 2024, **12**, 15601–15607.
46 N. Tanibata, K. Matsunoshita, H. Takeuchi, S. Akatsuka, M. Koga, H. Takeda and M. Nakayama, *J. Mater. Chem. A*, 2023, **11**, 25859–25864.
47 A. Hayashi, N. Masuzawa, S. Yubuchi, F. Tsuji, C. Hotehama, A. Sakuda and M. Tatsumisago, *Nat. Commun.*, 2019, **10**, 5266.
48 X. Feng, P. H. Chien, Z. Zhu, I. H. Chu and P. Wang, *Adv. Funct. Mater.*, 2019, **29**, 1807951.
49 Z. Zhang, E. Ramos, F. Lalère, A. Assoud, K. Kaup, P. Hartman and L. F. Nazar, *Energy Environ. Sci.*, 2018, **11**, 87–93.
50 Y. Ruan, F. Guo, J. Liu, S. Song, N. Jiang and B. Cheng, *Ceram. Int.*, 2019, **45**, 1770–1776.
51 S. Narayanan, S. Reid, S. Butler and V. Thangadurai, *Solid State Ionics*, 2019, **331**, 22–29.
52 L. Zhang, K. Yang, J. Mi, L. Lu, L. Zhao, L. Wang, Y. Li and H. Zeng, *Adv. Energy Mater.*, 2015, **5**, 1501294.
53 L. Wang, Z. Song, X. Lou, Y. Chen, T. Wang, Z. Wang, H. Chen, W. Yin, M. Avdeev, W. H. Kan and B. Hu, *Small*, 2024, **20**, 2400195.
54 T. Hakari, Y. Fujita, M. Deguchi, Y. Kawasaki, M. Otoyama, Y. Yoneda, A. Sakuda, M. Tatsumisago and A. Hayashi, *Adv. Funct. Mater.*, 2022, **32**, 2106174.